Choice of Reference Measurements Affects Quantification of Long Diffusion Time Behaviour Using Stimulated Echoes

Michiel Kleinnijenhuis,[1]* Jeroen Mollink,[1,2] Wilfred W. Lam,[1,3] Paul Kinchesh,[4] Alexandre A. Khrapitchev,[4] Sean C. Smart,[4] Saad Jbabdi,[1†] and Karla L. Miller[1†]

Purpose: To demonstrate how reference data affect the quantification of the apparent diffusion coefficient (ADC) in long diffusion time measurements with diffusion-weighted stimulated echo acquisition mode (DW-STEAM) measurements, and to present a modification to avoid contribution from crusher gradients in DW-STEAM.

Methods: For DW-STEAM, reference measurements at long diffusion times have significant b_0 value, because $b = 0$ cannot be achieved in practice as a result of the need for signal spoiling. Two strategies for acquiring reference data over a range of diffusion times were considered: constant diffusion weighting (fixed-b_0) and constant gradient area (fixed-q_0). Fixed-b_0 and fixed-q_0 were compared using signal calculations for systems with one and two diffusion coefficients, and experimentally using data from postmortem human corpus callosum samples.

Results: Calculations of biexponential diffusion decay show that the ADC is underestimated for reference images with $b > 0$, which can induce an apparent time-dependence for fixed-q_0. Restricted systems were also found to be affected. Experimentally, the exaggeration of the diffusion time–dependent effect under fixed-q_0 versus fixed-b_0 was in a range predicted theoretically, accounting for 62% (longitudinal) and 35% (radial) of the time dependence observed in white matter.

Conclusions: Variation in the b-value of reference measurements in DW-STEAM can induce artificial diffusion time dependence in ADC, even in the absence of restriction. **Magn Reson Med 79:952–959, 2018. © 2017 The Authors Magnetic Resonance in Medicine published by Wiley Periodicals, Inc. on behalf of International Society for Magnetic Resonance in Medicine. This is an open access article under the terms of the Creative Commons Attribution License, which permits use, distribution and reproduction in any medium, provided the original work is properly cited.**

Key words: stimulated echo; diffusion time; restriction; biexponential diffusion; apparent diffusion coefficient

INTRODUCTION

Dependence of the apparent diffusion coefficient (ADC) on diffusion time can reveal tissue properties with significance to neural health and disease. For instance, water molecules that are confined to a compartment exhibit reduced ADC with increased diffusion time. Long diffusion times can also probe membrane permeability. This dependence is often used in signal models that aim to improve biological specificity of diffusion MRI over nonspecific measures such as fractional anisotropy (1–7). To exploit these subtle changes in ADC, it is crucial that the measurements accurately reflect the diffusion propagator (ie, the displacement profiles over a range of diffusion times).

Diffusion time dependence has primarily been used to infer MRI measures of compartment size. Diffusion time dependence perpendicular to white matter tracts provides a marker of axon diameter, which has been proposed for improving tractography (8,9), estimating conduction velocity (10), and monitoring of disease status (11). Long diffusion time signals can also characterize the mesoscopic organization of tissue (5), providing markers for axonal varicosities (12), undulations (13), and white matter fiber dispersion (14,15). Finally, membrane permeability estimates based on diffusion time (6,16) are a potential biomarker of apoptosis (17), tissue composition (eg, myelination (18)), and tumor detection/classification (19–21).

Long diffusion time measurements face important technical challenges. Diffusion-weighted spin-echo (DW-SE) measurements experience T_2 signal loss that is intrinsically tied to long diffusion times and drastically reduces signal-to-noise ratio. Diffusion-weighted stimulated echo acquisition mode (DW-STEAM) (22) uncouples T_2 signal loss from diffusion time and therefore may be more appropriate for long diffusion time measurements.

In this note, we demonstrate the importance of the sequence parameters for DW-STEAM reference measurements, which are often referred to as $b = 0$, but in practice can have significant b-value for long diffusion times. In particular, we show that these reference measurements can have a major effect on estimated ADCs for systems that exhibit non-Gaussian diffusion, which is characteristic of all biological tissues. Crucially,

[1]Oxford Centre for Functional MRI of the Brain, University of Oxford, Oxford, United Kingdom.

[2]Department of Anatomy, Radboudumc, Nijmegen, The Netherlands.

[3]Sunnybrook Research Institute, University of Toronto, Toronto, Canada.

[4]Cancer Research UK & Medical Research Council Oxford Institute for Radiation Oncology, Department of Oncology, University of Oxford, Oxford, United Kingdom.

Grant sponsor: Wellcome Trust Senior research fellowship; Grant number: 091509/Z/10/Z (K.L.M.); Grant sponsor: MRC Career Development Fellowship; Grant number: MR/L009013/1 (S.J.); Grant sponsor: Cancer Research UK; Grant number: C5255/A15935 (A.A.K.).

*Correspondence to: Michiel Kleinnijenhuis, Ph.D., John Radcliffe Hospital (FMRIB), Headley Way, Oxford, OX3 9DU, United Kingdom. E-mail: michiel.kleinnijenhuis@ndcn.ox.ac.uk

Financial support provided by Nicola Sibson. The research was funded by the Wellcome Trust Senior research fellowship 091509/Z/10/Z (K.L.M.), MRC Career Development Fellowship MR/L009013/1 (S.J.), and Cancer Research UK C5255/A15935 (A.A.K.).

†These authors contributed equally to this work.

Received 27 October 2016; revised 16 February 2017; accepted 22 March 2017

DOI 10.1002/mrm.26711
Published online 3 May 2017 in Wiley Online Library (wileyonlinelibrary.com).

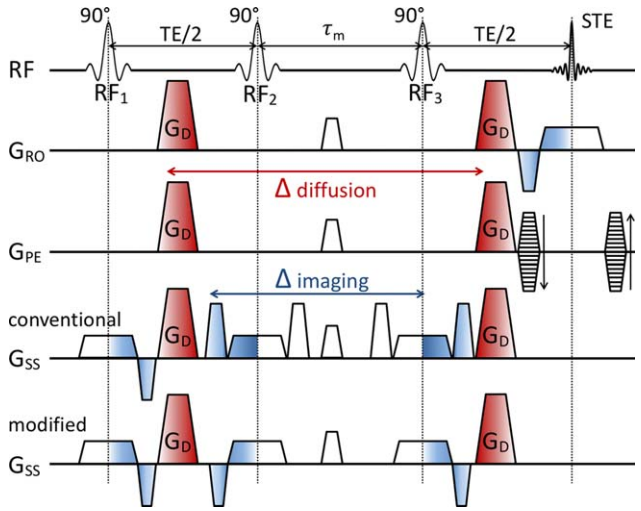

FIG. 1. DW-STEAM pulse sequence modification. The diffusion-weighting effect of the diffusion-encoding (red) and imaging gradients (blue) are indicated by color gradients. In the conventional scheme (fourth row), a pair of crushers is used on the slice-select axis to remove unwanted signal from the third RF pulse. These crushers (and half of the slice-select gradients) are separated by the mixing time τ_m, resulting in a substantial diffusion weighting at long diffusion times (see Supporting Fig. S1). This diffusion weighting—if not properly handled—results in considerable variation in *b*-value with diffusion time, as well as directional bias in the diffusion gradient directions (27). Because in the DW-STEAM sequence, the diffusion-encoding gradient already provides sufficient dephasing of the signal from RF3, the crushers are superfluous and can be replaced by usual slice-select refocussing. The modified scheme (bottom row) effectively removes the contribution of the imaging gradients that builds up during the mixing time by flipping the two crusher gradients to form pairs with the slice-select gradients to refocus the diffusion encoding outside of the mixing time. Adapted from Kinchesh et al. (28).

including the *b*-matrices in the ADC calculations is insufficient to draw valid conclusions about restrictions: The *b*-values of both the diffusion-weighted and reference measurements need to be kept constant over diffusion times.

THEORY

Diffusion Time Dependence of the ADC

In any diffusion-weighted sequence, varying the diffusion time (Δ) between diffusion-encoding gradients alters the diffusion-weighting *b* if other parameters are kept constant:

$$b = \gamma^2\delta^2G^2\left(\Delta - \frac{\delta}{3}\right) = q^2\left(\Delta - \frac{\delta}{3}\right). \quad [1]$$

Provided the displacement profile is Gaussian, diffusion measurements yield the same ADC, independent of the choice of *b* or Δ. However, with non-Gaussian diffusion (23–26), the choice of *b* is crucial for interpreting the diffusion time dependence of the ADC. For example, in biexponential diffusion—a simple departure from Gaussian diffusion—the ratio of a diffusion-weighted signal, S(Δ), and a reference measurement, $S_0(\Delta)$, is governed by

$$\frac{S(\Delta)}{S_0(\Delta)} = fe^{-bD_1} + (1-f)e^{-bD_2}. \quad [2]$$

In this scenario, varying Δ with constant *q* (varying *b*) induces an apparent dependence of the ADC on diffusion time. This diffusion time dependence occurs for any protocol in which $\log(S/S_0)$ is a nonlinear function of *b*, but would not be observed under constant *b* (varying $q = \gamma\delta G$). Crucially, the need for constant *b* holds for both diffusion-weighted *and* reference acquisitions with nonzero *b*-value. This is particularly important for DW-STEAM, in which reference measurements have significant *b*-value as a result of the configuration of crusher gradients.

DW-STEAM.

In DW-SE, the range of diffusion times that can be probed is limited by T_2 signal loss at long Δ. DW-STEAM (22) is an attractive alternative that stores magnetization along the longitudinal axis during the mixing time (τ_m) between the second and third 90° pulse (Fig. 1). DW-STEAM incurs a twofold signal reduction, but exhibits the much slower T_1 relaxation during τ_m.

However, in DW-STEAM the diffusion weighting from non-diffusion-encoding gradients can become substantial at long τ_m as a result of crushers that remove signal created by the third radiofrequency (RF) pulse (Fig. 1). In diffusion-weighted images, various strategies have been proposed to account for these gradients, including the use of the full *b*-matrix in analysis (29) and adapting the diffusion gradients (27). We propose a simple modification to the DW-STEAM sequence to reduce diffusion weighting from the crusher gradient (Fig. 1, bottom row). By negating the polarity of the crusher and slice-select gradients, the net gradient area is minimized during the mixing time. In the remainder of this work, we consider the effect of the residual gradient area in reference images on ADC quantification.

Reference Images with Varying Diffusion Times

Calculating the ADC necessitates a reference measurement to divide out the signal contributions unrelated to the diffusion gradients. For DW-STEAM, these contributions come from T_1 and T_2 decay. For measurements at multiple diffusion times, the variable T_1 decay during the mixing times requires a separate reference image for each Δ.

Unlike DW-SE, DW-STEAM reference measurements accumulate significant *b*-value at long diffusion times as a result of crusher gradients (Fig. 2a), which are smaller in amplitude than diffusion-encoding pulses, but otherwise have similar properties, including separation by the mixing time.

If the crusher gradient moment is kept constant over diffusion times (fixed-q_0), the associated *b*-value in the reference images (b_0) increases with diffusion time. An alternate design is to keep the b_0-value constant over diffusion times (fixed-b_0), which requires varying the crusher area, q_0. In this case, the minimum constant b_0-value over diffusion times is determined by b_0 at the longest diffusion time $b_{0,\Delta max}$.

It is instructive to compare the fixed-b_0 and fixed-q_0 approaches for mono- and biexponential decay, in which the latter is a representative deviation from Gaussian diffusion that is not driven by restriction. The ADC from a DW-STEAM experiment can be calculated from a two-point fit as (Fig. 2b)

$$ADC = \log(S/S_0)/(b - b_0). \quad [3]$$

For mono-exponential decay, this calculation yields the same ADC independent of b_0. When the decay is biexponential (Fig. 2b, dashed line), however, a two-point fit yields an ADC that decreases with increasing b_0 (Fig. 2b, dash-dotted lines). Therefore, fixed-q_0 designs yield an artificial time-dependence of the ADC as a result of the variation in b_0-value over diffusion times, which might be interpreted incorrectly as indicating restriction. Next we quantify this effect using simple simulations of unrestricted and restricted diffusion.

METHODS

ADC Calculations

The ADCs were compared between simulated measurements in which either b_0 or q_0 was held constant over diffusion times. For fixed-b_0, the $b_{0,\Delta max}$ was chosen as [10,20,30]% of the b-value of the diffusion-weighted images to reflect the range found in literature (12,19,27,30,31). The b_0-values are then

$$\begin{aligned} b_0(\Delta) &= b_{0,\Delta_{max}} && \text{for fixed-}b_0 \quad \text{and} \\ b_0(\Delta) &= {q_{0,\Delta_{max}}}^2(\Delta - \delta/3) && \text{for fixed-}q_0 \quad \text{where} \\ q_{0,\Delta_{max}} &= sqrt(b_{0,\Delta_{max}}/(\Delta_{max} - \delta/3)). \end{aligned} \quad [4]$$

First, we evaluated the signal with and without the sequence modification (Supporting Fig. S1). Second, we investigated the influence of reference measurements on ADC estimates of a biexponential signal model and a biophysical tissue model. All calculations assume infinitely narrow pulses. Signal calculations were performed using the MISST toolbox (32–34) that uses the matrix formalism (35) to compute the signal for arbitrary pulse sequences.

The biexponential signal model is characterized by diffusion coefficients D_s (slow) and D_f (fast) and volume fraction f_s. Biexponential decay was simulated for four fast diffusion coefficients relative to D_s, given by $D_f = [1,3,5,7] \times D_s$. The first case ($D_f = D_s$) represents mono-exponential diffusion. The fast volume fraction f_s was set to 0.33 in accordance with literature (36). Signal simulations were conducted to probe regimes of normalized diffusion time Δ/Δ_{max} and contrast $b \cdot D_s$ (b-value in terms of signal contrast for the slow diffusion coefficient).

The biophysical model is a simple two-compartment model with restricted intracellular diffusion in cylinders with radius r, diffusion coefficient D_i and volume fraction f_i, and hindered diffusion in the extracellular space with diffusion coefficient D_h. The evaluated ratios of the restricted and hindered diffusion coefficient were $D_h = [1,0.75,0.50,0.25] \times D_i$. D_i was set to 2 μm^2/ms and $f_i = 0.8$, in keeping with the fraction found in white matter tissue (37). Experimental regimes investigated for this model were $b = [0.0–8.5]$ ms/μm^2 perpendicular to the cylinders and $\Delta = [10–500]$ ms.

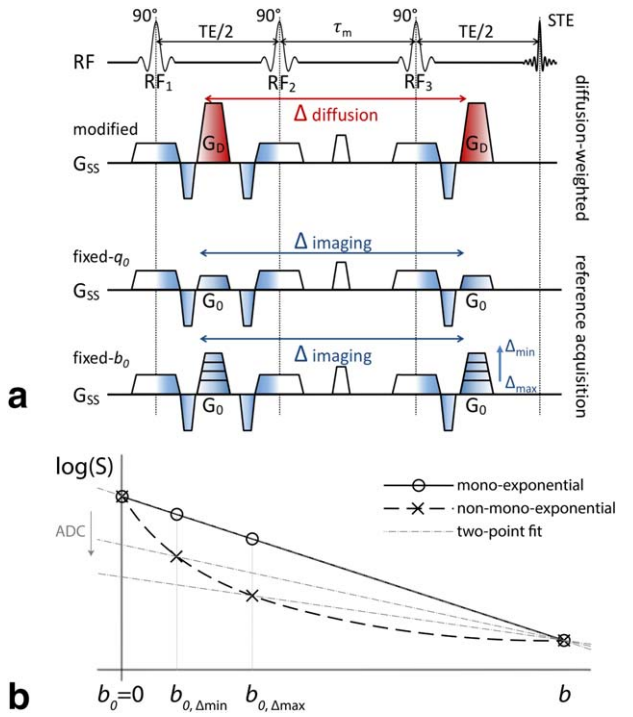

FIG. 2. Reference measurements in the DW-STEAM sequence. (**a**) DW-STEAM reference measurements in which the gradient $\mathbf{G}_0$ (fixed-q_0; third row) or the b_0-value are kept constant (fixed-b_0; fourth row). In the DW-STEAM sequence, the diffusion gradient ($\mathbf{G}_d$; second row) is used as an imaging gradient in the reference measurements (denoted $\mathbf{G}_0$; applied over all three axes) to crush the signal from the third RF pulse. In the b_0 image, the $\mathbf{G}_0$ is chosen according to the minimal q_0-value that achieves this, which might result in a nonnegligible b_0-value at long diffusion times. To obtain a constant b_0-value over diffusion times, the $\mathbf{G}_0$ needs to be increased for $\Delta < \Delta_{max}$ compared with the minimal value $G_{0,\Delta max}$. (**b**) ADC calculation of signals undergoing mono-exponential and non-mono-exponential decay. For mono-exponential decay (solid line), the behavior is linear in b, and any two-point fit of (b, b_0) yields the same ADC. For the non-mono-exponential, the slope of the linear fit, and thus ADC, decreases if the b_0-value increases over the measurements.

MRI Data Acquisition

Postmortem human corpus callosum samples from two brains provided by the Thomas Willis Brain Collection in Oxford were scanned. Coronal slabs of 5-mm thickness were cut at the level of the anterior commissure. From each slab, a 45 × 25 mm block was cut, including the medial corpus callosum and parts of the centrum semiovale, cingulate, and superior frontal gyri. The blocks were soaked in phosphate-buffered saline for 72 h and then transferred to a syringe filled with Fluorinert (3M, St. Paul, MN) 24 h before imaging.

MRI was performed on a 9.4 Tesla (T) 160-mm horizontal bore VNMRS preclinical scanner (Varian Inc, Corona, CA) with maximum gradient of 400 mT/m and a 26-mm ID quadrature birdcage coil (Rapid Biomedical GmbH, Germany).

DW-STEAM using a single-line readout was adapted to minimize the effect of imaging gradients on diffusion weighting (28). Measurements at eight diffusion times $\Delta = [70,100,150,200,250,300,350,400]$ ms were acquired using 30 directions distributed over the sphere. The repetition time (TR) was minimized for each diffusion time: TR = [2.4,2.4,2.4,2.4,2.4,2.6,3.6,4.1] s, with a minimum of 2.4 s to allow T_1 recovery between excitations (T_1 over our sample was estimated to be approximately 600 ms). The effective echo time was 16 ms. Five slices were acquired at 0.4 × 0.4 × 0.4 mm (matrix = 128 × 96; field of view = 51.2 × 38.4 mm). The complex data were resampled (matrix 64 × 48) and tapered with a Tukey window ($\alpha = 0.4$) to boost SNR and reduce Gibbs ringing.

The diffusion-weighted measurements used $b = 3.5$ ms·μm^{-2} with gradient duration $\delta = 2.22$ ms and variable gradient strength $|G| = 375$–157 mT/m for $\Delta = 70$–400 ms. For each Δ, two reference measurements were performed: one with constant $q_0 = 0.023$ μm^{-1} as the minimal value that adequately spoilt the signal generated from the third RF pulse (corresponding $b_0 = 0.117$–0.631 ms·μm^{-2}) and one with constant $b_0 = 0.631$ ms·μm^{-2} as the b_0 value with q_0 at $\Delta_{max} = 400$ ms.

MR Data Analysis

Diffusion tensors were fitted to the DW-STEAM data using FDT from FSL (38). The full *b*-matrix (ie, accounting for imaging gradients) was used to calculate the *b*-values and *b*-vectors. Tensor fitting was performed for each diffusion time separately, and for the two reference data sets separately (fixed-b_0 and fixed-q_0), while using the same diffusion-weighted measurements. Masks were created by thresholding two diffusion tensor metrics as follows: fractional anisotropy at > 0.20 for a white matter mask (which avoided including crossing-fiber voxels, such as in the centrum semiovale that had a lower fractional anisotropy); and mean diffusivity > 0.4 μm^2/ms for a gray matter mask. The diffusivities are presented for the longitudinal (the first eigenvalue) and radial (the average of the second and third eigenvalues) directions.

RESULTS

ADC Calculations

Figure 3a depicts mono-exponential modeling of unrestricted, biexponential diffusion for the fixed-b_0 and fixed-q_0 schemes, with constant high *b*-value across diffusion times and reference measurements with nonzero b_0-value. For fixed-b_0 (solid lines), the ADC is underestimated in comparison to a "true" $b_0 = 0$ ms/μm^2 (bold black line). Higher values for $b_{0,\Delta max}$ result in larger underestimation of the ADC. Nevertheless, fixed-b_0 does yield a *constant* ADC over diffusion times. The underestimation of the ADC also occurs for fixed-q_0 (dashed lines), but even more importantly, fixed-q_0 also induces an apparent diffusion time dependence in the absence of restriction, because the b_0-value increases with diffusion time.

The contour plot (Fig. 3b) quantifies, for an example regime $b_0/b = 0.2$ and $D_f = 5 \times D_s$, the difference between the ADCs calculated with fixed-q_0 and fixed-b_0 measurements expressed as a percentage of the "true" $b_0 = 0$ ms/μm^2 (ie, $(ADC_{fixed\text{-}q_0} - ADC_{fixed\text{-}b_0})/ADC_{b=0} \times 100\%$). At low *b*-values, the induced diffusion time dependence is small. However, a commonly used regime in experiments at long diffusion time, ie, $b \times D_s \approx [0.2$–$1.0]$ induces a large diffusion time dependence. The minimum b_0-value at the longest diffusion time and increasing difference in the biexponential signal components exacerbate the induced time dependence of the ADC (Supporting Fig. 2a). Conventional interpretations would incorrectly attribute the variation with diffusion time to

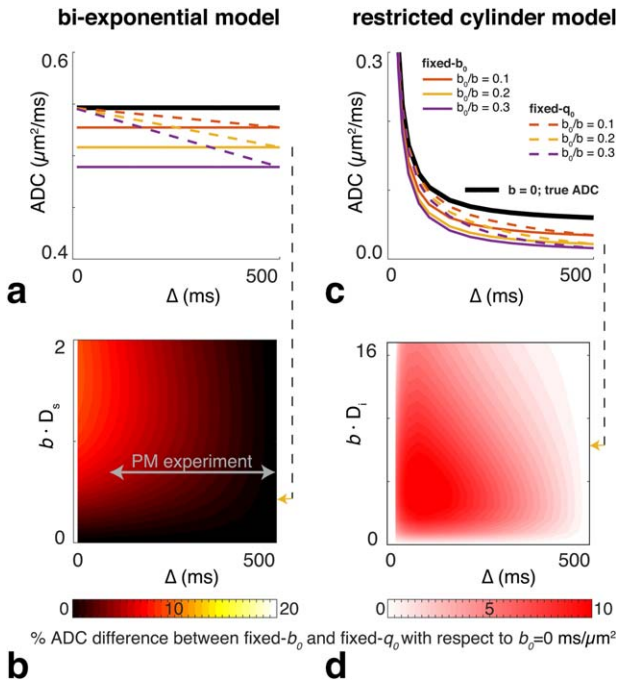

FIG. 3. The effect of reference measurements on the ADC. The biexponential model is shown on the left (**a, b**), and the restricted cylinder model is shown on the right (**c, d**). (**a, c**) The line plots show specific examples for measurements with fixed-q_0 (dashed lines) versus fixed-b_0 (solid lines). Lines of different color show the behavior for different b_0,Δmax values, where b_0,Δmax = [0, 10, 20, 30]% of the *b*-value. (**b, d**) The contour plots show differences in ADCs for the two reference measurement schemes; the color map represents the ADC difference between the fixed-q_0 ADC and the fixed-b_0 ADC as a percentage of the "true" ADC at $b_0 = 0$ ms/μm^2. (**a**) ADC behavior in biexponential signal model (without restriction) at $b \times D_s = 0.5$ ($b = 2.5$ ms·μm^{-2}; $D_s = 0.2$ μm^2·ms^{-1}, with $D_f = 5 \times D_s$ and $f_s = 0.3$. b)% ADC differences between fixed-b_0 and fixed-q_0 for the biexponential model for $D_f = 5 \times D_s$ and $b_0/b = 0.2$. (**c**) ADC behavior in the restricted cylinder model at $b = 4.0$ ms·μm^{-2}; $D_i = D_h = 2.0$ μm^2·ms^{-1}, with $r = 5$ μm and $f_i = 0.80$. d)% ADC differences between fixed-b_0 and fixed-q_0 for the restricted cylinder model for $D_i = D_h$ and $b_0/b = 0.2$. Note that the actual deviation from truth ($b_0 = 0$ ms/μm^2 measurement) is always maximal for fixed-b_0, because the b_0-value is determined by the longest diffusion time; however, our goal here is to quantify the difference between the two realistic measurement strategies: fixed-b_0 and fixed-q_0. The gray arrow indicates the regime of our postmortem measurements. All scales are linear. Supporting Figure S2 shows the effects of a different b_0/b ratios and different diffusion coefficient ratios. The effect of varying the intracellular volume fraction and the cylinder radius is provided in Supporting Figures S3 and S4, respectively.

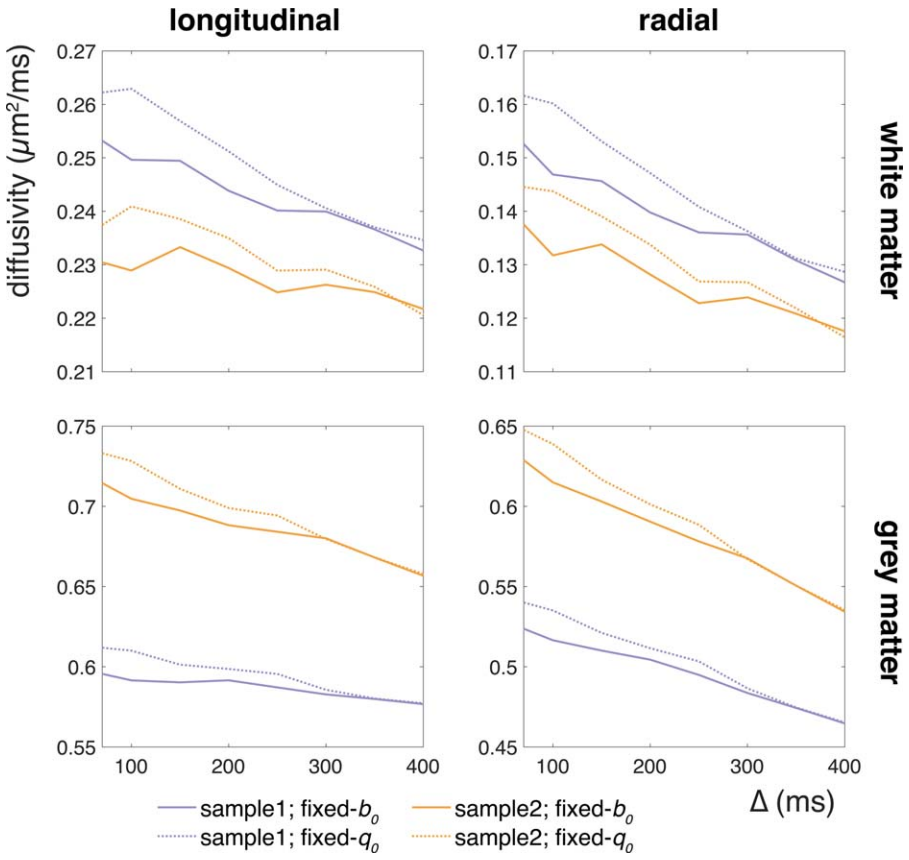

FIG. 4. Differences in the diffusion time dependence of the ADC with two normalization strategies (fixed-q_0 and fixed-b_0). Panels show the parallel (left column) and perpendicular (right column) diffusivities averaged over voxels in a white matter (top row) and gray matter (bottom row) mask. The two samples are plotted in different colors. The diffusivity decreases with diffusion time for all cases, but in each case is exaggerated when fixed-q_0 normalization is used. Note that the diffusivities for both reference image sets converge at the longest diffusion time where the b_0-values for both reference measurement strategies are equal (however, these correspond to separate acquisitions, and thus the measurements are not identical).

restriction, despite this being a fundamentally unrestricted system.

In the case of genuine restriction (Figs. 3c and 3d), ADC decreases are observed that are similar in magnitude to the biexponential model for the ratio's D_h/D_i that are common in these restriction models ($D_h = [0.5–1] \times D_i$). The differences between fixed-q_0 and fixed-b_0 decrease as the displacement profiles in the two compartments become more similar (eg, as D_h approaches the intracellular perpendicular ADC, as well as at short Δ where it even becomes negative as the diffusion in the intracellular space becomes free ($D_i > D_h$)) (Supporting Fig. 2b). For any nonzero b_0-value (both fixed-b_0 and fixed-q_0), the signal attenuation curves differ from the "true" $b_0 = 0$ ms/μm^2, ultimately affecting the estimation of the model parameters.

Postmortem MRI Data

Figure 4 depicts the diffusivities measured in two postmortem samples. Although the diffusivities differ between the samples, most likely because of differences in tissue preparation (39,40), they follow similar trends. Diffusivity decreases are observed with increasing diffusion time for both longitudinal and radial directions, as well as in different tissue types (white and gray matter). This diffusion time dependence is exaggerated when the signal is normalized by the fixed-q_0 measurement compared with the fixed-b_0 measurement: The slope for fixed-q_0 is larger than for fixed-b_0. Differences in diffusion time dependence between fixed-b_0 and fixed-q_0 are quantified in Table 1.

DISCUSSION

We demonstrate that the choice of acquisition parameters for the reference b_0-image is essential for interpreting ADC measurements using DW-STEAM. In a system that can be characterized by multiple diffusion coefficients, reference measurements with nonzero b-value lead to underestimation of the "composite" ADC. As this underestimation increases with b_0-value, the common approach of using a constant crusher gradient strength for the reference measurement at each diffusion time induces an artificial

Table 1
ADC Differences between Fixed-q_0 and Fixed-b_0 Strategies

ΔADC (%)	Fixed-q_0	Fixed-b_0	Fixed-q_0 effect
White matter longitudinal	7–11	4–8	44–80
White matter radial	19–20	15–17	35–35
Gray matter longitudinal	6–10	3–8	32–86
Gray matter radial	14–17	11–15	20–28

Note: The values in columns 1 and 2 indicate the difference in ADC between the short diffusion time ($\Delta = 70$ ms) and the long diffusion time measurement ($\Delta = 400$ ms), expressed as a percentage of the short diffusion time measurement. The third column shows the percentage of the ADC dependence as observed under fixed-b_0, which is added by dependence induced by fixed-q_0 measurements. The ranges indicate values for the two samples.

diffusion time dependence. Therefore, in experiments that rely on subtle variations of the ADC over a long interval of diffusion times, incorrect normalization could lead to misinterpretation of the results.

The size of this induced diffusion time dependence depends on the tissue's diffusion properties and the sequence parameters. In simulations, we demonstrated that stronger deviation from mono-exponential decay and a larger b_0-value for the reference measurement induces a larger diffusion time dependence. For typical acquisition parameters, the artificial effect can be on the order of the diffusion time dependence as a result of restrictions (Table 1, column 3). Data acquired from postmortem corpus callosum samples indicated that a considerable portion of the diffusion time dependence observed using fixed-q_0 references is consistent with multiple diffusion coefficients in the system. Nonetheless, the ADC still exhibited decreases with diffusion time under fixed-b_0 references, both perpendicular and parallel to the bundle, suggesting true restriction effects.

Although most studies investigating diffusion time dependence of ADC measures report a fixed *b*-value, reporting of the b_0-values in DW-STEAM is often omitted or inaccurate (ie, reported as $b = 0$ ms/μm^2 or "non-diffusion weighted"). The present investigation demonstrates that using the *b*-matrix is only sufficient to account for this effect when the underlying diffusion process is well characterized by a single diffusion coefficient. Both *b* and b_0 must be kept constant to draw conclusions about restriction. As a case in point, the use of fixed-b_0 measurements has changed our original interpretations of the data in Figure 4, which aimed to investigate diffusion time dependence along white matter fibers. There is not very strong evidence for a diffusion time dependence of the ADC in the longitudinal direction when a fixed-b_0 is used, whereas the fixed-q_0 data appear to suggest a small but consistent dependence.

In our simulations, a biexponential signal was generated to evaluate the effects of DW-STEAM reference measurements in the presence of non-Gaussian diffusion, which is well established in brain tissue (16). However, the choice of a biexponential system in our simulations is motivated by its simplicity and not to imply that this is the most appropriate tissue model. Our results extend to any form of non-mono-exponential signal decay.

The introduction of diffusion time dependence through variation in the *b*-values is limited to situations in which two-point fits are used to calculate a summary ADC from measurements with varying diffusion time. A model fit (eg, kurtosis (44), biexponential (45), CHARMED (46), AxCaliber (47)) to the nonnormalized data could be used to extract accurate and informative quantities from DW-STEAM measurements, although these models would have to be adapted to account for T_1 decay during the mixing time.

For models that rely on accurate estimation of ADC values (12,48), it becomes important to carefully consider the measurement regime, as not all regimes are equally affected. The exact sampling locations of the reference and diffusion-weighted measurements along the decay curve determine the extent of the induced diffusion time dependence. In the low-contrast regime, the effect is small: The linear extrapolation to the $b = 0$ ms/μm^2 intercept is reasonably accurate. Higher b_0-values for the reference measurement at the longest diffusion time spread the sampled points for fixed-q_0 design over a larger range of the decay curve, and therefore result in a larger induced diffusion time dependence (Fig. 2).

Although these effects were demonstrated in postmortem tissue, the results presented here should apply to in vivo data. Postmortem tissue has been shown to exhibit similar diffusion time dependence to in vivo tissue (49). Our measurements had a slight residual variation in the *b*-value with Δ and gradient direction ($b_{min} = 3.39$ ms·μm^{-2} at $\Delta = 70$ ms quadratically increasing to $b_{max} = 3.45$ ms·μm^{-2} at $\Delta = 400$ ms along the slice-select axis). Considering the relatively small size of the *b*-value variation in comparison to the b_0-variation and the use of the same diffusion-weighted data in both analyses, this does not invalidate our fixed-b_0 versus fixed-q_0 comparison and conclusions. Another remaining issue is the directional bias (27) caused by the particular direction of the diffusion weighting in the b_0-image, with respect to all directions in the shell. One solution for this would be to acquire a reference image for each direction and diffusion time at the cost of significant increase in scan time.

CONCLUSIONS

Future experiments with the DW-STEAM sequence using variable diffusion times should be designed to avoid variable *b*-values in the reference measurements to draw valid conclusions about quantities related to restriction, such as length scales and permeability. Incorporating the full *b*-matrix is insufficient: To avoid confounding the effects of restriction and possible multiple diffusion coefficients in the system under study, it is important to keep the *b*-value as well as the b_0-value constant over diffusion times. Unlike reference measurements with fixed-q_0, use of a constant b_0-value does not induce an apparent diffusion time dependence in the absence of restrictions. Fixed-b_0 is therefore preferable in experiments that draw conclusions from the relation between the ADC and diffusion time.

REFERENCES

1. Stanisz GJ, Szafer A, Wright GA, Henkelman RM. An analytical model of restricted diffusion in bovine optic nerve. Magn Reson Med 1997;37:103–111.
2. Assaf Y, Blumenfeld-Katzir T, Yovel Y, Basser PJ. AxCaliber: a method for measuring axon diameter distribution from diffusion MRI. Magn Reson Med 2008;59:1347–1354.
3. Alexander DC, Hubbard PL, Hall MG, Moore EA, Ptito M, Parker GJM, Dyrby TB. Orientationally invariant indices of axon diameter and density from diffusion MRI. NeuroImage 2010;52:1374–1389.
4. Lam WW, Jbabdi S, Miller KL. A model for extra-axonal diffusion spectra with frequency-dependent restriction. Magn Reson Med 2015; 73:2306–2320.
5. Novikov DS, Jensen JH, Helpern JA, Fieremans E. Revealing mesoscopic structural universality with diffusion. Proc Natl Acad Sci U S A 2014;111:5088–5093.
6. Latour LL, Svoboda K, Mitra PP, Sotak CH. Time-dependent diffusion of water in a biological model system. Proc Natl Acad Sci U S A 1994;91:1229–1233.
7. Lasič S, Nilsson M, Lätt J, Ståhlberg F, Topgaard D. Apparent exchange rate mapping with diffusion MRI. Magn Reson Med 2011; 66:356–365.

8. Sherbondy AJ, Rowe MC, Alexander DC. MicroTrack: an algorithm for concurrent projectome and microstructure estimation. Med Image Comput Comput Assist Interv 2010;13:183–190.
9. Girard G, Rutger Fick, Descoteaux M, Deriche R, Wassermann D. AxTract: microstructure-driven tractography based on the Ensemble Average Propagator. Inf Process Med Imaging 2015;24:675–686.
10. Horowitz A, Barazany D, Tavor I, Bernstein M, Yovel G, Assaf Y. In vivo correlation between axon diameter and conduction velocity in the human brain. Brain Struct Funct 2015;220:1777–1788.
11. Horowitz A, Tavor I, Hoffmann C, Miron S, Achiron A, Assaf Y. The in-vivo dynamics of axon diameter in multiple sclerosis. In Proceedings of the Annual Meeting of the Organization for Human Brain Mapping, Geneva, Switzerland; 2016. p 1232.
12. Fieremans E, Burcaw LM, Lee H-H, Lemberskiy G, Veraart J, Novikov DS. In vivo observation and biophysical interpretation of time-dependent diffusion in human white matter. NeuroImage 2016;129: 414–427.
13. Nilsson M, Lätt J, Ståhlberg F, van Westen D, Hagslätt H. The importance of axonal undulation in diffusion MR measurements: a Monte Carlo simulation study. NMR Biomed 2012;25:795–805.
14. Mollink J, Kleinnijenhuis M, Sotiropoulos SN, Ansorge O, Jbabdi S, Miller KL. Diffusion restriction along fibres: How coherent is the corpus callosum? In Proceedings of the 23rd Annual Meeting of ISMRM, Toronto, Canada; 2015. p 2783.
15. Kleinnijenhuis M, Mollink J, Kinchesh P, Lam WW, Galinsky VL, Frank LR, Smart SC, Jbabdi S, Miller KL. Monte Carlo diffusion simulations disambiguate the biophysical mechanisms of diffusion hinderance along tracts. In Proceedings of the 23rd Annual Meeting of the ISMRM, Toronto, Ontario, Canada; 2015. p 2756.
16. Van Zijl PC, Moonen CT, Faustino P, Pekar J, Kaplan O, Cohen JS. Complete separation of intracellular and extracellular information in NMR spectra of perfused cells by diffusion-weighted spectroscopy. Proc Natl Acad Sci U S A 1991;88:3228–3232.
17. Bailey C, Giles A, Czarnota GJ, Stanisz GJ. Detection of apoptotic cell death in vitro in the presence of Gd-DTPA-BMA. Magn Reson Med 2009;62:46–55.
18. Nilsson M, Lätt J, van Westen D, Brockstedt S, Lasič S, Ståhlberg F, Topgaard D. Noninvasive mapping of water diffusional exchange in the human brain using filter-exchange imaging. Magn Reson Med 2013;69:1573–1581.
19. Lampinen B, Szczepankiewicz F, van Westen D, Englund E, C Sundgren P, Lätt J, Ståhlberg F, Nilsson M. Optimal experimental design for filter exchange imaging: apparent exchange rate measurements in the healthy brain and in intracranial tumors. Magn Reson Med 2017;77:1104–1114.
20. Lasič S, Oredsson S, Partridge SC, Saal LH, Topgaard D, Nilsson M, Bryskhe K.Apparent exchange rate for breast cancer characterization. NMR Biomed 2016;29:631–639.
21. Teruel JR, Cho GY, Moccaldi RTM, Goa PE, Bathen TF, Feiweier T, Kim SG, Moy L, Sigmund EE. Stimulated echo diffusion tensor imaging (STEAM-DTI) with varying diffusion times as a probe of breast tissue. J Magn Reson Imaging 2017;45:84–93.
22. Merboldt KD, Hänicke W, Frahm J. Diffusion imaging using stimulated echoes. Magn Reson Med 1991;19:233–239.
23. Niendorf T, Dijkhuizen RM, Norris DG, van Lookeren Campagne M, Nicolay K. Biexponential diffusion attenuation in various states of brain tissue: implications for diffusion-weighted imaging. Magn Reson Med 1996;36:847–857.
24. Assaf Y, Mayk A, Cohen Y. Displacement imaging of spinal cord using q-space diffusion-weighted MRI. Magn Reson Med 2000;44:713–722.
25. Alexander DC, Barker GJ, Arridge SR. Detection and modeling of non-Gaussian apparent diffusion coefficient profiles in human brain data. Magn Reson Med 2002;48:331–340.
26. Jensen JH, Helpern JA, Ramani A, Lu H, Kaczynski K. Diffusional kurtosis imaging: the quantification of non-gaussian water diffusion by means of magnetic resonance imaging. Magn Reson Med 2005;53:1432–1440.
27. Basser PJ, Mattiello J, LeBihan D. MR diffusion tensor spectroscopy and imaging. Biophys J 1994;66:259–267.
28. Lundell H, Alexander DC, Dyrby TB. High angular resolution diffusion imaging with stimulated echoes: compensation and correction in experiment design and analysis. NMR Biomed 2014;27:918–925.
29. Kinchesh P, Kleinnijenhuis M, Miller KL, Smart S. Minimizing diffusion encoding of slice selection in stimulated echo imaging. In Proceedings of the 23rd Annual Meeting of ISMRM. Toronto, Canada; 2015. p 2791.
30. Clark CA, Le Bihan D. Water diffusion compartmentation and anisotropy at high b values in the human brain. Magn Reson Med 2000;44: 852–859.
31. Smith SM, Jenkinson M, Woolrich MW, et al. Advances in functional and structural MR image analysis and implementation as FSL. NeuroImage 2004;23:S208–S219.
32. D'Arceuil H, de Crespigny A. The effects of brain tissue decomposition on diffusion tensor imaging and tractography. NeuroImage 2007; 36:64–68.
33. Miller KL, Stagg CJ, Douaud G, et al. Diffusion imaging of whole, post-mortem human brains on a clinical MRI scanner. NeuroImage 2011;57:167–181.
34. Mollink J, Kleinnijenhuis M, Jbabdi S, Sotiropoulos SN, Ansorge O, Miller KL. Fiber dispersion in the corpus callosum revealed with postmortem diffusion weighted imaging and PLI. In Proceedings of the Annual Meeting of the Organization for Human Brain Mapping, Honolulu, HI; 2015. p 4103.
35. Kleinnijenhuis M, Mollink J, Kinchesh P, et al. Monte Carlo simulations disambiguate the biophysical mechanisms of diffusion hindrance along tracts. In Proceedings of the Annual Meeting of the Organization for Human Brain Mapping, Honolulu, HI; 2015. p 1769.
36. Lam WW, Miller KL, Kleinnijenhuis M, Jbabdi S. Longitudinally hindered diffusion of in vivo human white matter at long diffusion time. In Proceedings of the 23rd Annual Meeting of ISMRM. Toronto, Canada; 2015. p 2776.
37. Marschar AM, Kuder TA, Stieltjes B, Nagel AM, Bachert P, Laun FB. In vivo imaging of the time-dependent apparent diffusional kurtosis in the human calf muscle. J Magn Reson Imaging 2015;41:1581–1590.
38. Nilsson M, Lätt J, Nordh E, Wirestam R, Ståhlberg F, Brockstedt S. On the effects of a varied diffusion time in vivo: Is the diffusion in white matter restricted? Magn Reson Imaging 2009;27:176–187.
39. Assaf Y, Cohen Y. Assignment of the water slow-diffusing component in the central nervous system using q-space diffusion MRS: implications for fiber tract imaging. Magn Reson Med 2000;43:191–199.
40. De Santis S, Jones DK, Roebroeck A. Including diffusion time dependence in the extra-axonal space improves in vivo estimates of axonal diameter and density in human white matter. NeuroImage 2016;130: 91–103.
41. Burcaw LM, Fieremans E, Novikov DS. Mesoscopic structure of neuronal tracts from time-dependent diffusion. NeuroImage 2015;114:18–37.
42. Richardson S, Siow B, Panagiotaki E, Schneider T, Lythgoe MF, Alexander DC. Viable and fixed white matter: diffusion magnetic resonance comparisons and contrasts at physiological temperature. Magn Reson Med 2014;72:1151–1161.

SUPPORTING INFORMATION

Additional Supporting Information may be found in the online version of this article.

Fig. S1. DW-STEAM sequence modification efficacy. Resultant *b*-values for conventional and modified DW-STEAM sequence according to the post-mortem protocol are shown in the top row. All gradients were applied in the slice-select direction with the *b*-value from the diffusion gradient set to $b_{diff} = 3.5$, $b_{diff} = 0.7$ (fixed-b_0) and $b_{diff} = 0.0$ ms·μm^{-2} over all diffusion times, as well as one in which the gradient was kept constant over diffusion times (fixed-q_0). As measured in the (worst-case) direction along the slice-select axis, the conventional implementation of the DW-STEAM sequence results in a large range of *b*-values over the diffusion times in our postmortem protocol. The *b*-value accumulated from the imaging gradients alone is given by the blue line. The bottom row shows the ADC for conventional and modified DW-STEAM. For these calculations, we used values for the parameters of the biexponential signal model close to those found in our postmortem samples (ie, $D_s = 0.2$, $D_f = 1.0$; $f_s = 0.33$), as well as *q*-values for crusher and slice-select gradients representative for our postmortem MR protocol (ie, $q_c = q_s = 0.046\ \mu m^{-1}$). For the conventional sequence implementation, the undesired *b*-value variation implies considerable variation of the calculated ADC in the absence of restriction. The sequence modification, however, prevents the variation in *b*-value and results in a flat ADC over diffusion times if the *b*-value and b_0-value are constant. Next to demonstrating that the sequence modification is adequate, this indicates the importance of keeping the *b*-value and b_0-value of the diffusion-weighted images constant with diffusion time.

Fig. S2. Effect of reference measurements on the ADC. (a) Biexponential signal model (without restriction) with $f_s = 0.33$. (b) Restricted cylinder model with $D_i = 2\ \mu m^2/ms$, $f_i = 0.80$, and $r = 5\ \mu m$. In each panel, the columns show the results of different ratios of the diffusion coefficients in the respective models. The line plots in the top row of each panel show specific examples for measurements with fixed-q_0 (dashed lines) and fixed-b_0 (solid lines). Lines of different color show the behavior for different $b_{0,\Delta max}$

values, in which $b_{0,\Delta max}$ = [0, 10, 20, 30] % of the *b*-value. The three rows of contour plots show differences in ADCs for the two reference measurement schemes, where each row shows the results for a different b_0/b ratio. The color map represents the ADC difference between the fixed-q_0 ADC and the fixed-b_0 ADC as a percentage of the "true" ADC at $b_0 = 0$ ms/μm^2. The top row in (a) plots the ADC versus Δ curves for $b \times D_s = 0.5$ ($b = 2.5$ ms·μm^{-2}; $D_s = 0.2$ μm^2·ms^{-1}, with $D_f = 5 \times D_s$ and $f_s = 0.33$) (ie, representative of our postmortem experiment). A larger difference between diffusion coefficients leads to increased underestimation of the ADC (with respect to the "true" $b_0 = 0$ ms/μm^2), as does a larger b_0/b ratio. This is further quantified in the contour plots, where the effect of contrast parameter $b \times D_s$ can be examined. In (b) the top row shows the ADC versus Δ curves for $b = 4.0$ ms·μm^{-2}, with $r = 5$ μm and $f_i = 0.80$. Here, the difference between the fixed-b_0 and fixed-q_0 decreases with increasing difference between the compartment diffusion coefficients, because the intracellular compartment is highly restricted and the ADC_i is low. As D_h decreases, the compartmental ADCs are more similar and the differences between fixed-b_0 and fixed-q_0 diminish. For very short Δ, in which diffusion approaches free diffusion in the intracellular compartment, the % ADC difference measure becomes negative when $D_i > D_h$. Note that the actual deviation from truth ($b_0 = 0$ ms/μm^2 measurement) is always maximal for fixed-b_0, because the b_0-value is determined by the longest diffusion time; however, our goal here is to quantify the difference between the two realistic measurement strategies: fixed-b_0 and fixed-q_0. Different columns show the effect of a larger difference between the diffusion coeffiecients. The gray arrow indicates the regime of our postmortem measurements. All scales are linear. The effect of varying the intracellular volume fraction and the cylinder radius is provided in Supporting Figures S3 and S4, respectively.

Fig. S3. The effect of varying volume fraction on the ADC in the presence of multiple diffusion coefficients. (a) The ADC versus Δ curves (top row) and % ADC differences between fixed-b_0 and fixed-q_0 for the biexponential model with $D_f = 5 \times D_s$. The biexponential model exhibits high sensitivity to volume fraction variation, because it severely alters the ADC differences between the two pools (fast and slow). (b) ADC versus Δ curves (top row) and % ADC differences between fixed-b_0 and fixed-q_0 for the restricted cylinder model with $D_h = D_i$ and $r = 5$ μm. Although the volume fraction changes the ADC, the relative difference between fixed-b_0 and fixed-q_0 are found to be very similar.

Fig. S4. The effect of cylinder radius on the ADC in the presence of multiple diffusion coefficients in the restricted cylinder model.